International Journal of Geosciences, 2026, 17(8), 588-613
https://www.scirp.org/journal/ijg
ISSN Online: 2156-8367
ISSN Print: 2156-8359

Interpretable Prediction of Blast-Induced Rock Fragmentation Using Optimized Back Propagation Neural Networks and Support Vector Regression Models

Godwin Ativor[1]*, Susana Fosu Asamoah[1], Fred Arthur[1], Theophilus Asante Osei[1], Sheila Ayisi Mensah[1], Marlis Amonimah Codjoe[1], Clement Kweku Arthur[1], Ali Yusif[1], Solomon Evans Kweku Koomson[2]

[1]Mining Engineering Department, University of Mines and Technology, Tarkwa, Ghana
[2]Department of Sustainable Mineral Resource Development, University of Energy and Natural Resources, Sunyani, Ghana
Email: *gativor@umat.edu.gh

How to cite this paper: Ativor, G., Asamoah, S.F., Arthur, F., Osei, T.A., Mensah, S.A., Codjoe, M.A., Arthur, C.K., Yusif, A. and Koomson, S.E.K. (2026) Interpretable Prediction of Blast-Induced Rock Fragmentation Using Optimized Back Propagation Neural Networks and Support Vector Regression Models. *International Journal of Geosciences*, **17**, 588-613.
https://doi.org/10.4236/ijg.2026.178028

Received: July 13, 2026
Accepted: August 23, 2026
Published: August 26, 2026

Abstract

Reliable prediction of blast-induced rock fragmentation is essential for optimizing blasting performance, reducing operational costs, and improving the efficiency of downstream mining operations. This study develops and evaluates hybrid machine learning models by integrating Backpropagation Neural Network (BPNN) and Support Vector Regression (SVR) with three optimization algorithms, namely the Zebra Optimization Algorithm (ZOA), Grey Wolf Optimizer (GWO), and Bayesian Optimization (BO). The resulting hybrid models, ZOA-BPNN, GWO-BPNN, BO-BPNN, ZOA-SVR, GWO-SVR, and BO-SVR, were compared with their standalone counterparts using the Mean Absolute Error (MAE), Mean Squared Error (MSE), Correlation Coefficient (R), and Coefficient of Determination (R^2). Among the developed models, ZOA-BPNN achieved the highest predictive performance, with a validation MAE of 0.021, MSE of 0.046, R of 0.992, and R^2 of 0.984. Model interpretation using SHapley Additive exPlanations (SHAP) identified powder factor as the most influential variable governing fragment size, followed by charge per hole, charge length, and bench height, thereby providing valuable insights for blast design optimization. Overall, the results demonstrate that integrating metaheuristic optimization with machine learning substantially enhances prediction accuracy and robustness, with ZOA-BPNN emerging as the most effective framework for intelligent prediction and decision support in surface mine blasting.

Keywords

Rock Fragmentation, Metaheuristic Optimization, Zebra Optimization Algorithm, Back Propagation Neural Network, Support Vector Regression

1. Introduction

Blasting remains central to mining, tunneling, and civil construction, since it is the primary means of breaking rock masses for excavation, loading, and processing [1]-[3]. Despite advances in explosives and detonation technology, only about 20% - 30% of the released energy actually fragments and displaces rock [4] [5]; the rest escapes as seismic waves and air shock, producing flyrock, ground vibration, air overpressure, and backbreak [6]-[10]. These side effects raise safety and environmental concerns and add cost through operational delays and equipment damage.

Fragment size governs almost everything downstream. Well-sized fragments load and haul faster, protect crushers, and cut grinding energy, so blast quality is a direct lever on productivity and cost [11] [12]. Oversized boulders demand secondary breaking, while excess fines waste processing capacity and wear out equipment faster. Accurately predicting and controlling fragment size distribution is therefore central to running a cost-effective operation.

Fragmentation prediction has moved through several generations of models built on field data, expert judgment, and statistics [13]-[17]. Cunningham [18] [19] introduced the Kuz-Ram model, which combines the Rosin-Rammler distribution with empirical relationships to estimate mean fragment size (X_{50}) and uniformity (n) from explosive and rock-mass parameters. It remains widely used for its simplicity but has long been criticized for inaccuracy. Lawal [20] refined it using image analysis, striking a better balance between accuracy and practicality. The Crush Zone Model and Two-Component Model, developed at the Julius Kruttschnitt Mineral Research Centre [21] [22], added mechanisms for the fines generated near the borehole, and the Swebrec function [23] [24] later gave a better fit across the full-size range, feeding into the Kuznetsov-Cunningham-Ouchterlony (KCO) model [25]. Fragmentation-energy fan and percentile-based models extended this further [26] [27].

Even so, empirical models rest on fixed assumptions and site-specific calibration, so they generalize poorly to new conditions [28]. Traditional models such as the Kuznetsov equation [29] and Kuz-Ram [18] [19] were fitted to limited datasets and assume largely linear relationships, which cannot capture the non-linear interactions that actually govern fragmentation [30]-[32], and they were calibrated over narrow ranges of blast parameters [33]. The Swebrec function corrected some of Rosin-Rammler's known weaknesses in underestimating fines and coarse fragments [23] [26] and gave a better S-shaped fit across the size spectrum [28], but it still depends on predetermined parameters that cannot flex with changing blast and geological conditions. This limitation, common to every empirical approach, is what motivates the machine learning approach used here.

Machine learning has become an attractive alternative for the same reason empirical models fall short: machine learning models can model complex, non-linear systems with many interacting variables, and larger datasets have made this practical [34]-[37]. In mining, AI already supports air overpressure and ground vibration prediction and production scheduling [38]-[40], as well as equipment condition monitoring [41]-[43]. Among these techniques, Back Propagation Neural Network (BPNN) and Support Vector Regression (SVR) are widely used for fragmentation prediction because they handle non-linear, multi-dimensional data well [44] [45] and have proven flexible and robust across mining and geotechnical applications [46]-[49]. Each still has a weakness, however: BPNN training is sensitive to weight initialization and network architecture, which risks overfitting, slow convergence, or entrapment in local minima [50], while SVR generalizes well on small or high-dimensional data but depends heavily on kernel and regularization choices that are usually tuned by trial and error [51].

This study addresses both weaknesses by pairing BPNN and SVR with metaheuristic optimizers, in two stages. First, the best baseline configuration is identified for each learner: BPNN is tested with Levenberg-Marquardt, Scaled Conjugate Gradient, and Bayesian Regularization training algorithms, while SVR is tested with linear, Gaussian, and polynomial kernels. Second, the Zebra Optimization Algorithm (ZOA), Grey Wolf Optimization (GWO), and Bayesian Optimization (BO) are applied to search for the best internal parameters of each baseline model, removing the guesswork of manual tuning and improving convergence and generalization.

The three optimizers were chosen because they search in different ways. ZOA mimics zebra herd behavior, specifically how zebras move collectively and evade predators, balancing broad exploration with local refinement [52]. GWO mimics the hunting hierarchy of grey wolves, using a structured pursue-and-encircle strategy well suited to fine-tuning a model's core parameters [53]. BO takes a different, model-based approach by constructing a probabilistic surrogate of the objective function and using it to identify promising parameter combinations with relatively few computationally expensive evaluations [54].

This study develops and benchmarks, for the first time, six hybrid models, namely ZOA-BPNN, GWO-BPNN, BO-BPNN, ZOA-SVR, GWO-SVR, and BO-SVR, against their unoptimized counterparts, all implemented in MATLAB. To enhance model transparency and support engineering decision-making, the study further employs SHapley Additive exPlanations (SHAP), a model-agnostic interpretability technique derived from cooperative game theory that quantifies the contribution of each input variable to model predictions. SHAP provides both global feature importance and insight into how individual blasting parameters influence predicted fragmentation outcomes, thereby improving the interpretability and practical applicability of the developed models. Finally, the comparative evaluation provides practical insights into optimizer-model compatibility, demonstrating that the effectiveness of a metaheuristic algorithm depends not only on its optimization capability but also on its interaction with the underlying machine learning model. These contributions provide a more reliable, transparent, and interpretable framework for intelligent blast-induced rock fragmentation prediction.

The rest of the paper is organized as follows. Section 2 reviews related hybrid modelling studies. Section 3 describes the study site, and Section 4 the dataset. Sections 5 and 6 present the modelling methodology and model development process. Section 7 reports and discusses the results, including SHAP-based interpretability, and Section 8 concludes with implications and directions for future work.

2. Related Studies on Hybrid Machine Learning Fragmentation Models

This section reviews hybrid machine learning approaches used to predict blast-induced rock fragmentation, to position the present study within current research. A systematic search of ScienceDirect and Google Scholar used terms such as "rock fragmentation," "metaheuristic optimization," "hybrid machine learning," and "blasting prediction." Studies were retained only if they combined a machine learning model with a metaheuristic optimizer for fragmentation prediction, and only if published between 2015 and 2025.

Table 1 summarizes the resulting studies, their hybrid techniques, base models, optimizers, and reported performance. Notably, few of these studies first benchmark different learning functions within the standalone model before applying metaheuristic optimization—a gap this study addresses directly.

Table 1. A review of hybrid models for predicting blast-induced rock fragmentation.

Reference	Year	Hybrid Model	Key Findings/Outcome
Yu *et al.* [55]	2025	AHA-GPR	High generalizability across different mine sites (Chilean copper mine and Indian coal mine), R^2 up to 0.990.
Zhao *et al.* [56]	2025	RF-BOA, ERT-BOA, GBoost-BOA, AdaBoost-BOA	Best-performing model (GBoost-BOA) achieved R^2 of 0.960.
Zheng *et al.* [57]	2023	LSSVM-BFO, LSSVM-AFSA, LSSVM-APSO	LSSVM-BFO yielded the highest performance ($R^2 = 0.9960$).
Yari *et al.* [58]	2023	JSO-LightGBM	Achieved excellent accuracy on test data ($R^2 = 0.996$).
Huang *et al.* [59]	2022	CSO-linear, PSO-linear, CSO-power, PSO-power	CSO-power achieved the lowest error (RMSE = 0.847).
Fang *et al.* [60]	2021	FFA-BGAM	Using 136 blast images, accurately predicted rock size distribution ($R^2 = 0.980$).
Zhou *et al.* [61]	2019	ANFIS-FFA, ANFIS-GA	Based on 88 blasting events, ANFIS-GA achieved excellent performance ($R^2 = 0.989$).

Continued

Hasanipanah *et al.* [62]	2018	ANFIS-PSO	Demonstrated strong capability ($R^2 = 0.890$), outperforming SVM and standard ANFIS.
Murlidhar *et al.* [63]	2018	ICA-ANN	High accuracy ($R^2 = 0.949$) in testing for fragmentation prediction.
Ebrahimi *et al.* [64]	2016	ABC-ANN	Using field data, optimized blasting parameters to improve fragmentation (RMSE = 2.760).

JSO: Jellyfish Search Optimizer; LSSVM: Least Squares Support Vector Machine; AFSA: Artificial Fish Swarm Algorithm; APSO: Adaptive Particle Swarm Optimization; RF: Random Forest; ERT: Extremely Randomized Trees; AHA: Artificial Hummingbird Algorithm; GBoost: Gradient Boosting; AdaBoost: Adaptive Boosting; ANN: Artificial Neural Network; ABC: Artificial Bee Colony; ANFIS: Adaptive Neuro-Fuzzy Inference System; PSO: Particle Swarm Optimization; GA: Genetic Algorithm; FFA: Firefly Algorithm; BGAM: Boosted Generalized Additive Model; CSO: Cat Swarm Optimization; GPR: Gaussian Process Regression; LightGBM: Light Gradient Boosting Machine; BFO: Bacterial Foraging Optimization; BOA: Bayesian Optimization Algorithm; ICA: Imperialist Competitive Algorithm.

3. Site Description

The mine lies in one of Ghana's most productive gold belts, about 10 km southwest of Tarkwa, 70 km from Sekondi, and 320 km from Accra. Geologically, it sits within the Tarkwaian Group of the West African Craton, made up mainly of metavolcanic and metasedimentary rocks from the Birimian Supergroup [65] (**Figure 1**). Operations follow a standard open-pit sequence of drilling, blasting, loading, and haulage, with blasting typically conducted daily unless delayed by weather or other operational factors. The mine operates several production drill rigs, including Rock Commander, Epiroc SmartROC T45, Epiroc DML, and Sandvik drill rigs. However, the dataset analyzed in this study was obtained from production blasts drilled primarily using Sandvik drill rigs with hole diameters of 115 mm and 127 mm, depending on the ground conditions. Accordingly, the descriptive statistics presented in **Table 2** reflect only the hole diameters represented in the analyzed dataset.

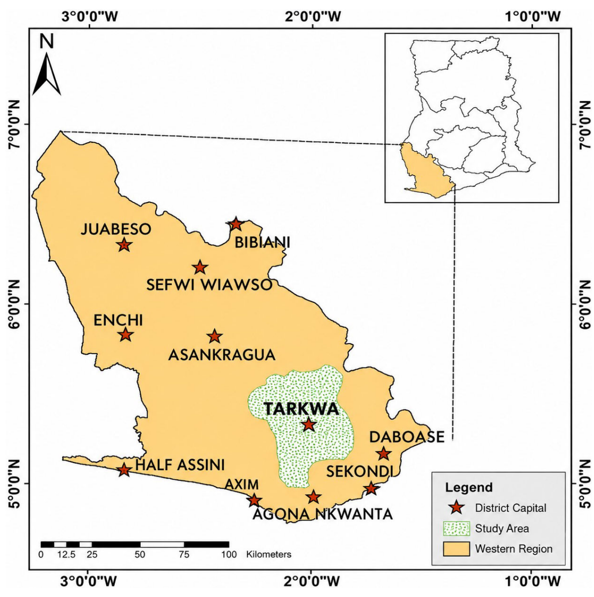

Figure 1. Study area.

4. Data Description

A total of 498 blasts were monitored at the mine, with data recorded across three parameter groups: blast design, explosive characteristics, and rock properties. Blast design parameters—spacing (S), burden (B), initial and final stemming height (IS, FS), bench height (H), and charge length (L), all in meters, plus hole diameter (D) in millimeters—were measured alongside explosive parameters: charge per hole (C, kg) and powder factor (PF, kg/m^3). Powder factor was calculated as charge per hole divided by blast volume, where blast volume is the product of burden, spacing, and bench height ($PF = C/(B \times S \times H)$, kg/m^3). Rock properties were represented by uniaxial compressive strength (UCS, MPa). These ten parameters served as the independent variables, with the actual mean fragment size (X_{50}, cm) as the dependent variable. Mean fragment size (X_{50}) for each blast was determined using WipFrag image-analysis software applied to digital images of the resulting muckpile, captured immediately after each blast across the full pile to ensure representative coverage. Oversized fragments that could not be reliably delineated within the image frame were handled using WipFrag's boulder-tracing function to correct the size distribution. Table 2 summarizes the dataset statistically.

Table 2. Statistical overview of the rock fragmentation dataset.

Parameter	Category	Maximum	Std. Dev	Mean	Minimum
Burden (m)	Input	4.0	0.089	3.76	3.5
Spacing (m)		5.0	0.221	3.86	3.5
Uniaxial Compressive Strength (MPa)		288.7	55.017	253.06	168.3
Bench Height (m)		12.0	1.653	8.322	6
Hole Diameter (mm)		127.0	4.554	117.09	115
Initial Stemming Height (m)		3.5	0.294	3.05	2.3
Final Stemming Height (m)		3.1	0.284	2.65	1.9
Charge Length (m)		9.5	1.463	6.25	1.7
Charge per Hole (kg)		113.0	19.302	77.87	20.0
Powder Factor (kg/m^3)		0.9	0.161	0.65	0.25
Mean Fragment Size (cm)	Output	115.6	7.372	34.40	13.55

Figure 2 shows the Pearson correlation matrix, used to quantify linear relationships among the input variables and X50. Bench height correlates strongly with charge length ($R \approx 0.98$) and charge per hole ($R \approx 0.96$), and initial and final stemming height are perfectly correlated ($R = 1.00$); hole diameter also correlates with both stemming heights ($R \approx 0.71$), and charge length with charge per hole ($R \approx 0.94$). Against X_{50}, bench height, stemming heights, charge length, and charge per hole all show moderate positive correlation—coarser blast designs tend to produce coarser fragments, while powder factor shows a strong negative correlation ($R \approx -0.85$), confirming its dominant role in controlling fragment size. This matches expected blasting mechanics: more explosive energy per unit volume breaks rock finer.

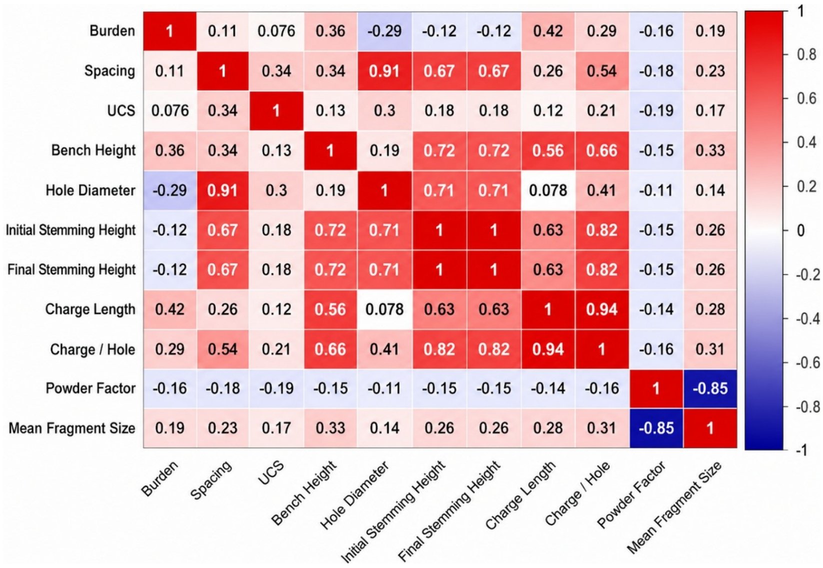

Figure 2. Illustration of Pearson correlation plot.

Figure 3 shows the Spearman rank correlation, which captures monotonic relationships without assuming linearity—a useful check given the non-linear interactions typical of blasting data. The Spearman results largely confirm the Pearson findings, with initial and final stemming height again perfectly correlated (ρ = 1.00) and both strongly linked to charge per hole (ρ ≈ 0.85); bench height also correlates strongly with IS, FS, and C (ρ ≈ 0.76). The inverse relationship between powder factor and X50 is even stronger here (ρ ≈ −0.95), confirming that this effect holds consistently across both linear and non-linear analysis.

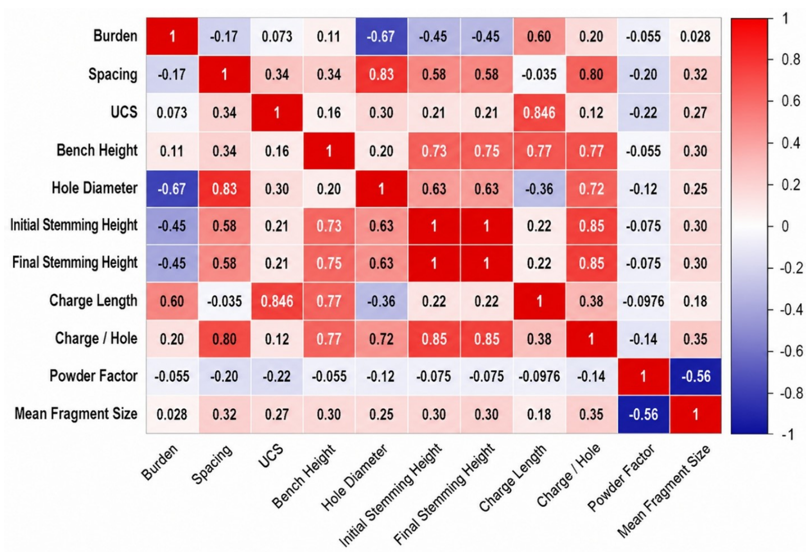

Figure 3. Illustration of Spearman correlation plot.

5. Methodology

5.1. Backpropagation Neural Network

Backpropagation Neural Networks (BPNN) are a simple, effective type of feedforward network [66] [67], made up of an input layer, one or more hidden layers, and an output layer. Each neuron computes a weighted sum of its inputs, adds a bias, and passes the result through an activation function, as shown in Equation (1) [68].

$$y_j = f\left(\sum_{i=1}^{n}\left(w_{ij} \times x_i\right) + b_j\right) \tag{1}$$

where the values at the nodes in the previous layer (*i*) and the layer currently active (*j*) are illustrated by x_i and y_j, respectively. The total nodal values obtained from the previous layer are depicted by *n*. The network's biases and weights are denoted by b_j and w_{ij}.

For this study, a tangential hyperbolic function was utilized based on its ability to produce more precise outcomes. The function's range is bounded by −1 and 1, and its mathematical expression is given in Equation (2) as:

$$y_j = f\left(net\right) = 2 \times \left(\frac{1}{e^{-2.net} + 1} - 0.5\right) \tag{2}$$

The network's final output (y_j) is calculated by feeding the computed internal network value (*net*) through an activation function (*f*). During the training phase, weights and biases values are repeatedly adjusted to minimize the error between the predicted network values and the actual target values This mechanism is essentially a minimization problem [69]. For this study, the BPNN model was built and executed using MATLAB 2023a software. For a deeper look at how the BPNN works, comprehensive details on the BPNN itself are available in resources like the work presented by Jain *et al.* [70].

5.2. Support Vector Regression

Support Vector Regression (SVR) is a variant of the Support Vector Machine adapted for regression tasks. As Zhang and O'Donnell [71] note, its structure is not fixed in advance—the input vectors that define it are determined during training. For a training set with input vector x and target f, the SVR estimator *f*(*x*) is given in Equation (3), where w is the weight vector, *b* the bias, and *K*(*x*) a non-linear basis function mapping the input into a higher-dimensional space.

$$f\left(x\right) = b + w \cdot \left(\kappa\left(x\right)\right) \tag{3}$$

where weight vector $w = \left(w_1, w_2, w_3, \cdots, w_z\right)$, the bias term is *b,* and the basis function vector $\kappa\left(x\right) = \left(\kappa_1\left(x_1\right), \cdots, \kappa\left(x_z\right)\right)$ referring to a series of non-linear changes. The non-linear basis function is used to convert the *R*-dimensional input vector from a low-dimensional phase to a high-dimensional space $\kappa\left(x\right)$. Support Vector Regression (SVR) aims to identify the optimal separating hyperplane that enhances the model's capacity to learn from data and effectively address a given problem [72]. Solving Equation (3) necessitates the use of Equation (4), while adhering to the constraints outlined in Equation (5). It is important to highlight that the structure of an SVR is not fixed in advance; rather, the input variables that contribute to the model are typically selected throughout the training process.

$$\underset{w,b,\xi,\xi^*}{\text{minimize}} \ \frac{1}{2}[\![w]\!]^2 + M \cdot \sum_{J=1}^{Z}\left(\xi_j + \xi_j^*\right) \tag{4}$$

$$\text{s.t.}\begin{cases} \left(b + w^{\mathrm{T}}\kappa\left(x_j\right)\right) - y_j \le \varepsilon - \xi_j \\ b + w^{\mathrm{T}}\kappa\left(x_j\right) - y_j \le \xi_j^* + \varepsilon \\ \xi_j^*, \xi_j \ge 0 \end{cases} j = 1, 2, \cdots, Z \tag{5}$$

where the positive trade-off parameters, ε and *M*, regulate the measured deviation scale in maximization, while the slack factors ξ and ξ^* resolve the errors using the expression in Equation (5).

Support Vector Regression (SVR) relies on kernel functions, which function similarly to activation functions by implicitly projecting input data into a higher-dimensional space to enable better separation of classes. To construct accurate and efficient models, commonly used SVR kernels were evaluated, including the linear kernel, Gaussian kernel, and polynomial kernel functions [73]. These are represented by the following mathematical expressions, respectively.

$$K\left(x, \overline{x}\right) = x^T \cdot \overline{x} \tag{6}$$

$$G\left(x, \overline{x}\right) = \exp\left(\gamma \left\|-x + \overline{x}\right\|^2\right) \tag{7}$$

$$P\left(x, \overline{x}\right) = \left(c + \left(x^T \cdot \overline{x}\right)\right)^q \tag{8}$$

where *x*, $\overline{x}$ represents the input feature vectors, $x^T \cdot \overline{x}$ is the product of the vectors γ is the scaling factor, c is the coefficient term, and $-x + \overline{x}$ refers to the Euclidean distance between two vectors.

5.3. Zebra Optimization Algorithm

Metaheuristic algorithms draw on natural behaviors to solve complex optimization problems [52]. The Zebra Optimization Algorithm (ZOA) used here is a swarm-based method known for fast convergence, modelled on how zebra herds forage and evade predators together, balancing broad exploration with local refinement.

5.4. Grey Wolf Optimization

The Grey Wolf Optimizer (GWO) mimics the social hierarchy and hunting behavior of grey wolves [53] and is widely used across engineering and machine learning [74]. It identifies the three best solutions (α, β, δ) as leaders that guide the remaining wolves toward the global optimum, through three phases: encircling, hunting, and attacking the prey.

5.5. Bayesian Optimization

Bayesian Optimization (BO) uses a probabilistic surrogate model, typically a Gaussian Process, to approximate an expensive or complex objective function [75], rather than evaluating it directly many times. The surrogate gives a mean estimate and an uncertainty at each point, and BO uses this to choose where to sample next by maximizing an acquisition function, balancing exploration of new regions against exploitation of known good ones [75] [76].

6. Model Development

This section outlines the data preprocessing, formulation of the baseline models, the metaheuristic optimization procedures used to develop the hybrid predictive models, and the SHAP-based interpretation approach adopted to explain the influence of the input variables on model predictions.

6.1. Data Preprocessing

The complete dataset was randomly divided into a training dataset (80%) and a validation dataset (20%). The training dataset was used for model development and hyperparameter optimization. During model development, five-fold cross-validation was performed exclusively within the training dataset to identify the optimal model configurations and hyperparameters. In each fold, normalization parameters were computed (using Equation 9) only from the corresponding training subset and subsequently applied to the associated validation fold without refitting, thereby preventing information leakage. After model development, the final models were evaluated using the independent validation dataset, which was not involved in the training or hyperparameter optimization process [77].

$$N_i = \left\{ \frac{2}{(s_{\max} - s_{\min})} \times (s_i - s_{\min}) \right\} - 1 \tag{9}$$

where, the normalized data point of variable s_i is represented by N_i, the maximum scores are defined by $s_{\max}$, and the minimum scores of the measured samples are indicated by $s_{\min}$.

6.2. Baseline Model Formulation

The baseline BPNN and SVR models were developed by evaluating multiple candidate learning strategies and selecting the best-performing configurations. For the BPNN, three training algorithms, namely Levenberg-Marquardt (LM), Scaled Conjugate Gradient (SCG), and Bayesian Regularization (BR), were investigated. The number of hidden neurons was varied from 1 to 150 to determine the optimal network architecture. Model performance was evaluated using the Mean Absolute Error (MAE), Mean Square Error (MSE), correlation coefficient (R), and coefficient of determination (R^2). The training algorithm and network architecture that produced the lowest prediction errors and highest goodness-of-fit metrics on the validation dataset were selected as the baseline BPNN model.

For the SVR, three kernel functions, namely Linear, Polynomial, and Gaussian, were evaluated. The kernel yielding the best predictive performance was selected as the baseline model. The principal SVR hyperparameters, including the regularization parameter (C), kernel parameter (σ), and insensitive loss parameter (ε), were subsequently considered for optimization to further improve predictive performance.

6.3. Hybrid Model Development and Hyperparameter Optimization

The selected baseline BPNN and SVR models were subsequently integrated with the Zebra Optimization Algorithm (ZOA), Grey Wolf Optimizer (GWO), and Bayesian Optimization (BO) to improve predictive accuracy through optimal hyperparameter selection. For the BPNN, the optimization algorithms searched for the optimal network weights and biases, whereas for the SVR they optimized the regularization parameter (C), kernel parameter (σ), and insensitive loss parameter (ε). The objective function was defined as the mean squared error (MSE) computed over the training folds.

The optimization variables were normalized within the interval [−1, 1] to maintain a compact search space, improve computational efficiency, and achieve a balanced trade-off between exploration and exploitation. The preliminary experiments were conducted to identify ranges that consistently produced stable convergence while avoiding unnecessary computational cost. For ZOA, the population size varied from 10 to 120 zebras with iteration numbers ranging from 100 to 1500. The swapping probability (P_s) and exploration constant (C) were fixed at 0.5. For GWO, the population size ranged from 1 to 50 wolves, while the maximum number of iterations varied between 10 and 150 for the BPNN and between 10 and 200 for the SVR. Bayesian Optimization employed a Gaussian Process surrogate model with a Matérn kernel, using 5 to 50 initial sampling points and 50 to 400 optimization iterations. Expected Improvement and Upper Confidence Bound acquisition functions guided the search for the optimal solution.

Each optimization algorithm iteratively updated candidate solutions until the maximum number of iterations or the convergence criterion was satisfied. The optimal parameter set identified by each optimization algorithm was then used to retrain the corresponding BPNN or SVR model. The optimized models were subsequently evaluated using the validation dataset, while the training dataset was used for model development and optimization. Figure 4 presents the overall model development and optimization framework. All simulations were performed on an HP laptop equipped with an AMD Ryzen 5 processor and 12 GB of RAM.

6.4. SHAP-Based Model Formulation

To enhance the interpretability of the developed machine learning framework, SHapley Additive exPlanations (SHAP) [78] were employed to quantify the contribution of each input variable to model predictions. SHAP is a model-agnostic interpretability technique derived from cooperative game theory that assigns each feature a Shapley value, representing its average marginal contribution to the prediction across all possible combinations of input variables. Unlike conventional feature importance measures, SHAP provides both the magnitude and direction of each feature's influence, thereby offering consistent and locally accurate explanations of model behavior.

Following model development and performance evaluation, SHAP analysis was performed on the model that demonstrated the highest predictive performance. Global feature importance was quantified using the mean absolute SHAP values computed from all observations in the validation dataset, allowing the relative influence of each blasting parameter on fragment size prediction to be ranked. In addition, SHAP summary plots were generated to illustrate how variations in individual input variables influenced the predicted fragmentation outcomes.

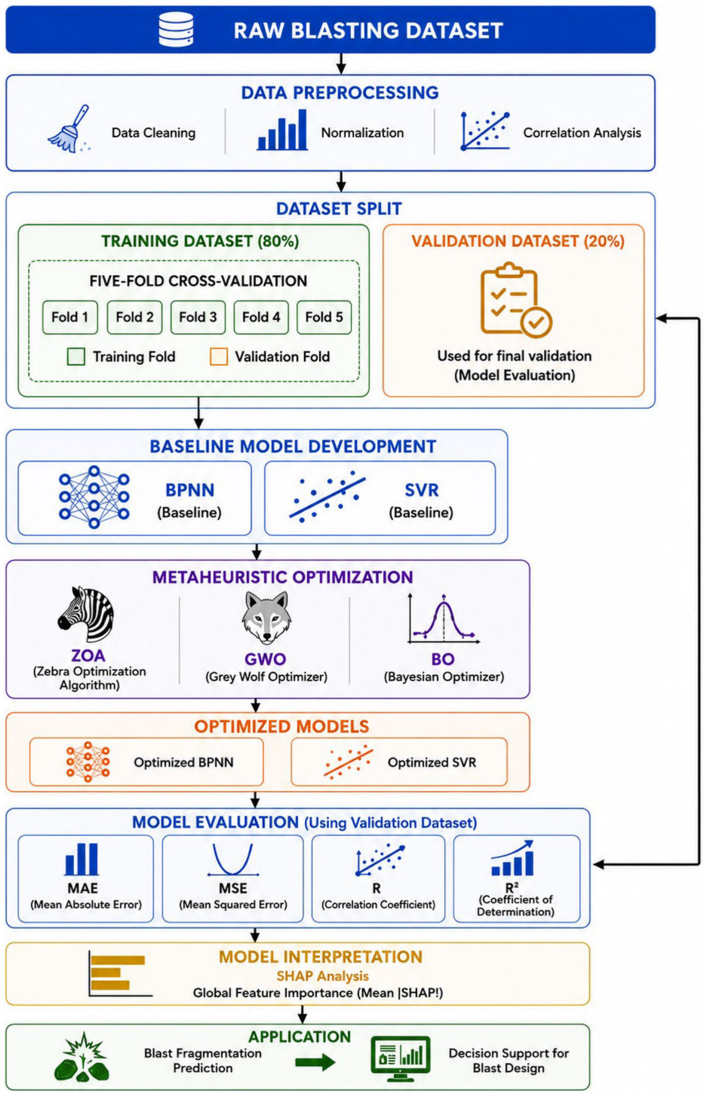

Figure 4. Conceptual framework of BPNN and SVR models integrated with optimization algorithms for blast-induced rock fragmentation prediction.

6.5. Model Performance Evaluation

Model performance was assessed using MAE, MSE, correlation coefficient (R), and coefficient of determination (R^2), which together capture prediction accuracy, error magnitude, and fit. Lower MAE and MSE indicate better accuracy, while higher R and R^2 indicate stronger agreement between predicted and observed values. These metrics are defined in Equations. (10)-(13) [79]-[81], where OF and PF denote the observed and predicted fragment sizes, their subscripted averages denote the dataset means, and n is the total number of samples.

$$\text{MAE} = \frac{1}{n} \times \sum_{i=1}^{n} \left| OF_i - PF_i \right| \tag{10}$$

$$\text{MSE} = \frac{1}{n} \times \sum_{i=1}^{n} \left(OF_i - PF_i \right)^2 \tag{11}$$

$$\text{R} = \frac{\sum_{i=1}^{n} \left(OF_i - OF_{av} \right)\left(PF_i - PF_{av} \right)}{\sqrt{\sum_{i=1}^{n} \left(OF_i - PF_{av} \right)^2} \times \sqrt{\sum_{i=1}^{n} \left(PF_i - PF_{av} \right)^2}} \tag{12}$$

$$\text{R}^2 = 1 - \left(\frac{\sum_{i=1}^{n} \left(OF_i - PF_i \right)^2}{\sum_{i=1}^{n} \left(OF_i - OF_{av} \right)^2} \right) \tag{13}$$

In the statistical equations, OF_i and PF_i denote the observed and predicted fragment sizes for the i-th sample, respectively. The terms OF_{av} and PF_{av} represent the mean values of the observed and predicted fragment sizes across the entire dataset. The total number of samples used for model development is designated by n.

7. Results and Discussion

This section presents the results of the modelling process: first the baseline training algorithms and kernel functions with their hyperparameter settings, then the comparative performance of the optimized hybrid models, followed by feature importance and the broader implications of the findings.

7.1. Developed Models

Table 3 shows that all three BPNN training algorithms exhibited good generalization, with training performance consistently outperforming validation performance by a small margin. This pattern indicates effective learning while maintaining good generalization to unseen data, with no evidence of overfitting. Among the evaluated algorithms, Bayesian Regularization achieved the best overall performance, recording the lowest training MAE (0.362) and MSE (0.781), together with the highest R (0.836) and R^2 (0.698). Its validation performance remained consistently strong (MAE = 0.389, MSE = 0.853, R = 0.812, and R^2 = 0.659), demonstrating superior predictive capability and robust generalization compared with the Levenberg-Marquardt and Scaled Conjugate Gradient algorithms. Consequently, Bayesian Regularization was selected as the baseline BPNN training algorithm for subsequent hybrid optimization.

Table 3. Statistical analysis results of the training algorithms modelled in the BPNN.

Training Algorithm	Phase	MAE	MSE	R	R^2
Levenberg Marquardt	Training	0.521	1.982	0.782	0.611
	Validation	0.548	2.064	0.766	0.587
Scaled Conjugate Gradient	Training	0.641	1.274	0.812	0.658
	Validation	0.673	1.351	0.791	0.626
Bayesian Regularization	**Training**	**0.362**	**0.781**	**0.836**	**0.698**
	Validation	**0.389**	**0.853**	**0.812**	**0.659**

Table 4 shows a similar pattern for the SVR models, with all three kernel functions exhibiting slightly better performance during training than during validation. The small differences between the two phases indicate good generalization ability while suggesting that the models did not overfit the training data. Among the evaluated kernels, the Gaussian kernel demonstrated the best overall performance, achieving the lowest training MAE (2.035) and MSE (4.612), together with the highest R (0.615) and R^2 (0.378). Its validation performance remained comparably strong (MAE = 2.127, MSE = 4.831, R = 0.592, and R^2 = 0.350), confirming its superior predictive capability and robustness compared with the Linear and Polynomial kernels.

Table 4. Statistical performance of candidate SVR kernel functions.

Kernel	Phase	MAE	MSE	R	R^2
Linear	Training	2.932	5.018	0.56	0.314
	Validation	3.041	5.226	0.535	0.286
Gaussian	**Training**	**2.035**	**4.612**	**0.615**	**0.378**
	Validation	**2.127**	**4.831**	**0.592**	**0.350**
Polynomial	Training	2.581	4.891	0.580	0.336
	Validation	2.681	5.064	0.557	0.310

Based on these results, Bayesian Regularization and the Gaussian kernel were selected as the baseline BPNN training algorithm and SVR kernel, respectively. These baseline models were subsequently optimized using the Zebra Optimization Algorithm (ZOA), Grey Wolf Optimizer (GWO), and Bayesian Optimization (BO). The optimization variables were bounded within the interval [−1, 1] to maintain a compact search space, improve computational efficiency, and achieve a balanced trade-off between exploration and exploitation during the optimization process. The reported values correspond to the optimal solution returned by each optimization algorithm. **Table 5** presents the baseline model architectures together with the optimal hyperparameter settings for each optimization algorithm.

Table 5. Baseline model architecture and optimal hyperparameter configurations for the optimization algorithms integrated with the BPNN and SVR models.

Algorithm	Hyperparameter	Optimized BPNN	Optimized SVR
Baseline BPNN	Hidden layer architecture	Single hidden layer	–
	Number of hidden neurons	46	–
	Hidden-layer activation function	tansig	–
	Output-layer activation function	purelin	–
	Training algorithm	Bayesian Regularization	–
	Maximum training epochs	1000	–
	Performance function	Mean Squared Error (MSE)	–
Baseline SVR	Kernel function	–	Gaussian (RBF)
	Regularization parameter (C)	–	11.2
	Epsilon (ε)	–	0.07
	Kernel scale (σ)	–	3.4
ZOA	Population size (zebras)	110	70
	Maximum iterations	800	600
	Swapping probability (P_s)	0.5	0.5
	Exploration constant (C)	0.5	0.5
GWO	Population size (wolves)	40	50
	Maximum iterations	100	200
	Leadership adjustment factor	0.7	0.5
BO	Initial sample points	25	30
	Maximum iterations	300	350

7.2. Statistical Comparison of Optimized Models

Table 6 compares the training and validation performance of the baseline models and their optimized hybrid counterparts.

Table 6. Training and validation performance of the baseline and optimized models.

Optimized Model	Phase	MAE	MSE	R	R^2
BPNN	Training	0.362	0.781	0.836	0.698
	Validation	0.389	0.853	0.812	0.659
ZOA-BPNN	**Training**	**0.018**	**0.041**	**0.994**	**0.988**
	Validation	**0.021**	**0.046**	**0.992**	**0.984**
GWO-BPNN	Training	0.039	0.089	0.901	0.792
	Validation	0.044	0.095	0.891	0.776

Continued

BO-BPNN	Training	0.163	0.361	0.933	0.870
	Validation	0.175	0.386	0.922	0.849
SVR	Training	2.035	4.612	0.615	0.378
	Validation	2.127	4.831	0.592	0.350
ZOA-SVR	Training	0.029	0.066	0.927	0.859
	Validation	0.033	0.072	0.914	0.837
GWO-SVR	Training	1.352	3.011	0.669	0.448
	Validation	1.409	3.129	0.644	0.416
BO-SVR	Training	0.811	1.794	0.781	0.610
	Validation	0.856	1.885	0.764	0.584

Among all the evaluated models, ZOA-BPNN demonstrated the best predictive performance, achieving a validation MAE of 0.021, MSE of 0.046, R of 0.992, and R^2 of 0.984. These results indicate that the model explained approximately 98.4% of the variability in rock fragmentation, highlighting its excellent predictive accuracy and strong generalization capability. The superior performance of ZOA-BPNN can be attributed to the complementary strengths of the Zebra Optimization Algorithm and the BPNN. Conventional BPNN training relies on gradient-based optimization, which is susceptible to premature convergence and local optima. In contrast, ZOA combines effective global exploration with local exploitation, enabling a more comprehensive search of the network's weight and bias space. By optimizing the initial weights and biases before training, ZOA provided a more favorable starting point for the learning process, thereby reducing convergence to poor local solutions, improving model stability, and enhancing prediction accuracy. The validation coefficient of determination (R^2) results presented in **Figure 5** further support these findings, with ZOA-BPNN exhibiting the highest R^2 value among all the developed models. GWO-BPNN and BO-BPNN also outperformed the standalone BPNN, increasing the coefficient of determination from 0.659 to 0.776 and 0.849, respectively. These improvements demonstrate the effectiveness of metaheuristic optimization in enhancing the predictive capability of neural network models, although neither algorithm matched the optimization efficiency achieved by ZOA. Among the support vector regression models, the standalone SVR produced the lowest predictive performance, with a validation MAE of 2.127 and an R^2 of 0.350. Nevertheless, integrating SVR with metaheuristic algorithms substantially improved its performance. ZOA-SVR emerged as the strongest SVR-based model, achieving a validation MAE of 0.033 and an R^2 of 0.837. This result further demonstrates the robustness and adaptability of ZOA, indicating that its optimization capability extends beyond neural networks to kernel-based learning algorithms.

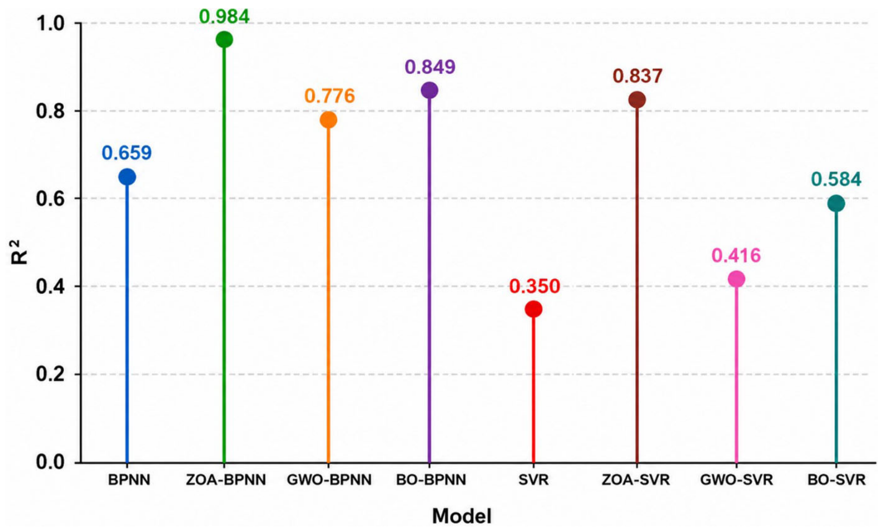

Figure 5. Comparison of coefficient of determination results of the applied models.

7.3. Model Ranking

To provide a comprehensive comparison of the developed models, the validation results were ranked using the four evaluation metrics, namely MAE, MSE, R, and R^2. For MAE and MSE, lower values indicate superior predictive performance and were therefore assigned higher rankings. Conversely, for R and R^2, higher values indicate stronger predictive capability and received higher rankings. Each model was ranked from 1 (best) to 8 (worst) for each metric, and the individual rankings were summed to obtain an overall score. Consequently, a lower total score represents better overall model performance. This ranking approach enables simultaneous consideration of prediction accuracy, goodness-of-fit, and model reliability, thereby facilitating an objective comparison of the standalone and hybrid intelligent models. Table 7 ranks all eight models across the four metrics.

Table 7. Overall ranking of the developed intelligent models based on validation performance.

Model	MAE	MSE	R	R^2	Total score	Rank
ZOA-BPNN	**1**	**1**	**1**	**1**	**4**	**1**
ZOA-SVR	2	2	3	3	10	2
BO-BPNN	4	4	2	2	12	3
GWO-BPNN	3	3	4	4	14	4
BPNN	5	5	5	5	20	5
BO-SVR	6	6	6	6	24	6
GWO-SVR	7	7	7	7	28	7
SVR	8	8	8	8	32	8

The ranking confirms that ZOA-BPNN was the best-performing model, achieving first place across all four evaluation metrics with the lowest overall score of 4.

ZOA-SVR ranked second, followed by BO-BPNN, demonstrating that the Zebra Optimization Algorithm consistently produced the greatest performance improvements irrespective of the underlying learning algorithm. GWO-BPNN also outperformed the standalone BPNN, while BO-SVR and GWO-SVR showed substantial improvements over the conventional SVR model. Among the baseline models, BPNN ranked fifth and considerably outperformed the standalone SVR, which placed last. These findings demonstrate that integrating metaheuristic optimization with machine learning models substantially enhances predictive performance, although the magnitude of improvement depends on the compatibility between the optimization algorithm and the underlying predictive model.

7.4. SHAP-Based Interpretation of Feature Influence on Fragmentation Prediction

Following the comparative evaluation of all developed models, the ZOA-BPNN model demonstrated the highest predictive performance and was therefore selected for SHAP-based interpretation. Figure 6 presents the SHAP summary plot, which ranks the blasting parameters according to their mean absolute SHAP values and illustrates both the magnitude and direction of each variable's influence on the predicted fragment size.

Powder factor emerged as the most influential predictor by a substantial margin, exhibiting the widest range of SHAP values (approximately −15 to +25). Higher powder factor values consistently shifted the predictions towards smaller fragment sizes, confirming its dominant role in controlling blast fragmentation. This finding is consistent with established blasting theory, where increasing the explosive energy per unit rock volume generally enhances rock breakage and produces finer fragmentation.

The SHAP feature importance plot (Figure 7) further corroborates these findings, ranking charge per hole and charge length as the second and third most influential variables, with mean absolute SHAP values of approximately 0.325 and 0.230, respectively. Bench height followed with a mean absolute SHAP value of approximately 0.194, while the remaining variables contributed comparatively less to the model predictions. Collectively, these results indicate that explosive energy distribution and blast geometry are the principal factors governing fragmentation performance.

It is important to note that, in this study, the blast design variables exhibit strong correlations, as demonstrated by the Pearson and Spearman analyses. In particular, powder factor, charge per hole, charge length, bench height, and the stemming variables are operationally related and jointly define the distribution of explosive energy within a blast. Consequently, their SHAP values should be interpreted within the context of these interdependent blasting parameters rather than as completely independent effects. Despite these correlations, the consistent identification of powder factor as the dominant predictor reinforces its critical influence on fragment size prediction and supports the robustness and engineering reliability of the developed ZOA-BPNN model.

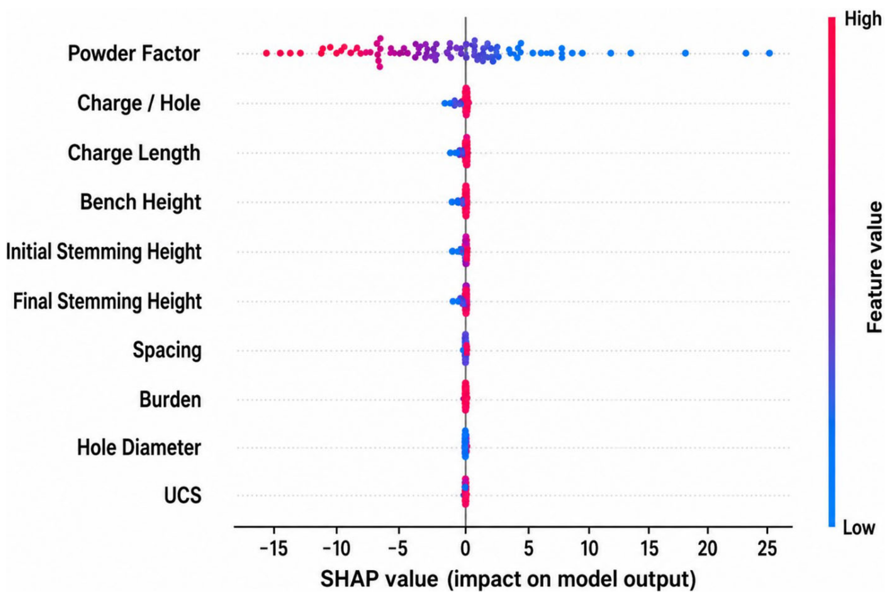

Figure 6. SHAP summary plot showing global feature influence.

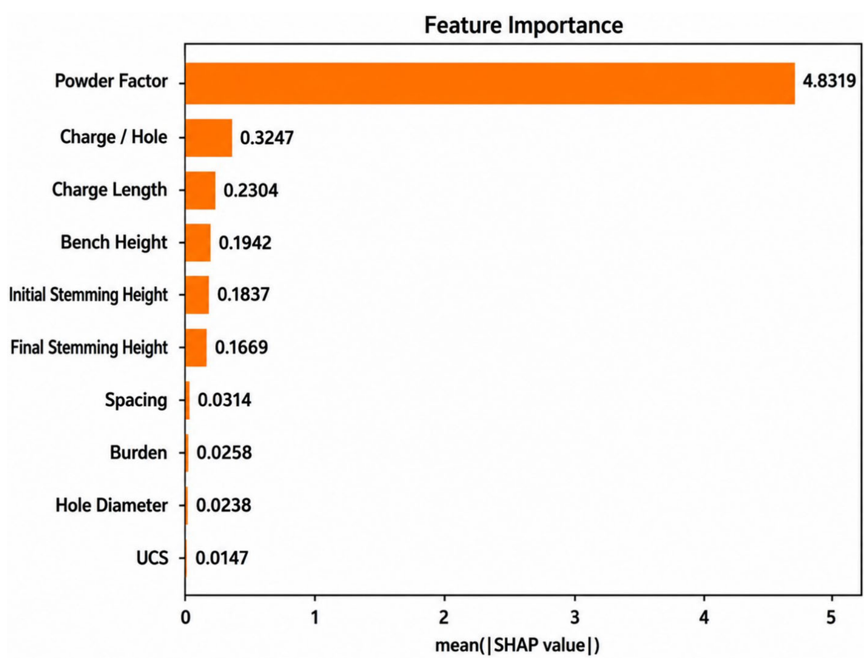

Figure 7. Mean absolute SHAP value bar chart for feature importance ranking.

8. Conclusions and Future Proposals

This study developed and evaluated hybrid machine learning models for predicting blast-induced rock fragmentation by integrating BPNN and SVR with the Zebra Optimization Algorithm (ZOA), Grey Wolf Optimizer (GWO), and Bayesian Optimization (BO). The results demonstrate that metaheuristic optimization significantly improved the predictive performance of both machine learning models compared with their standalone counterparts. Among the developed models, ZOA-BPNN achieved the best performance, attaining a validation MAE of 0.021, MSE of 0.046, R of 0.992, and R^2 of 0.984, thereby explaining approximately 98.4% of the variability in fragment size. ZOA-SVR also performed well, while BO-BPNN and GWO-BPNN provided competitive alternatives.

SHAP analysis identified powder factor as the most influential predictor, followed by charge per hole, charge length, and bench height, confirming that explosive energy distribution and blast geometry are the primary factors controlling fragmentation. These findings enhance the interpretability of the developed models and provide practical guidance for blast design optimization.

Although the proposed framework demonstrated excellent predictive capability, the study was based on data from a single mine and did not explicitly consider additional rock mass characteristics and blast sequencing variables. Future research should validate the models using multi-mine datasets, incorporate additional geological and operational parameters, and extend the framework into intelligent real-time decision-support systems for surface mine blasting.

Conflicts of Interest

The authors declare no conflicts of interest regarding the publication of this paper.

References

[1] Wang, B., Xu, H., Zhang, Q., Shen, Z. and Jin, Y. (2025) Experimental Study on the Mechanism of Rockburst in Tunnel Construction by Drilling and Blasting Construction in High Ground Stress Stratum. *Scientific Reports*, **15**, Article No. 8914. https://doi.org/10.1038/s41598-025-93551-y

[2] Xu, P., Yang, R., Zuo, J., Ding, C., Chen, C., Guo, Y., *et al.* (2022) Research Progress of the Fundamental Theory and Technology of Rock Blasting. *International Journal of Minerals, Metallurgy and Materials*, **29**, 705-716. https://doi.org/10.1007/s12613-022-2464-x

[3] Zhou, J., Zhang, Y. and Qiu, Y. (2024) State-of-the-Art Review of Machine Learning and Optimization Algorithms Applications in Environmental Effects of Blasting. *Artificial Intelligence Review*, **57**, Article No. 5. https://doi.org/10.1007/s10462-023-10636-8

[4] Inanloo Arabi Shad, H., Sereshki, F., Ataei, M. and Karamoozian, M. (2018) Investigation of the Rock Blast Fragmentation Based on the Specific Explosive Energy and *In-Situ* Block Size. *International Journal of Mining and Geo-Engineering*, **52**, 1-6.

[5] Ding, C., Yang, R., Zhu, X., Feng, C. and Zhou, J. (2023) Rock Fracture Mechanism of Air-Deck Charge Blasting Considering the Action Effect of Blasting Gas. *Tunnelling and Underground Space Technology*, **142**, Article ID: 105420. https://doi.org/10.1016/j.tust.2023.105420

[6] Ziggah, Y.Y., Temeng, V.A. and Arthur, C.K. (2023) A New Synergetic Model of Neighbourhood Component Analysis and Artificial Intelligence Method for Blast-Induced Noise Prediction. *Modeling Earth Systems and Environment*, **9**, 3483-3502. https://doi.org/10.1007/s40808-023-01719-0

[7] Mohammadi Azizabadi, H.R., Mansouri, H. and Fouché, O. (2014) Coupling of Two Methods, Waveform Superposition and Numerical, to Model Blast Vibration Effect on Slope Stability in Jointed Rock Masses. *Computers and Geotechnics*, **61**, 42-49. https://doi.org/10.1016/j.compgeo.2014.04.008

[8] Zhou, J., Asteris, P.G., Armaghani, D.J. and Pham, B.T. (2020) Prediction of Ground Vibration Induced by Blasting Operations through the Use of the Bayesian Network and Random Forest Models. *Soil Dynamics and Earthquake Engineering*, **139**, Article ID: 106390. https://doi.org/10.1016/j.soildyn.2020.106390

[9] Zhang, J., Zhou, C., Zhang, X., Jiang, N., Sheng, Z. and Jianmin, H. (2024) Prediction of Rock Fragmentation Using the Genetic Algorithm to Optimize Extreme Learning Machine. *Mining, Metallurgy & Exploration*, **41**, 3023-3039. https://doi.org/10.1007/s42461-024-01064-5

[10] Li, E., Zhang, Z., Zhou, J., Khandelwal, M., Yu, Z. and Monjezi, M. (2025) Indirect Hazard Evaluation by the Prediction of Backbreak Distance in the Open Pit Mine Using Support Vector Regression and Chicken Swarm Optimization. *Geohazard Mechanics*, **3**, 1-14. https://doi.org/10.1016/j.ghm.2024.11.001

[11] Ozdemir, K. (2021) Evaluation of Blast Fragmentation Effects on Jaw Crusher Throughput. *Arabian Journal of Geosciences*, **14**, Article No. 2036. https://doi.org/10.1007/s12517-021-08426-z

[12] Khodayari, A., Xu, C., Dare-Bryan, P., Dowd, P., Lapcevic, V. and Metcalfe, A. (2026) Impact of Blast Design Parameters on Rock Fragmentation in Sub-Level Caving: A Multivariate Regression Approach. *Journal of Rock Mechanics and Geotechnical Engineering*, **18**, 3348-3364. https://doi.org/10.1016/j.jrmge.2025.07.038

[13] Aler, J. and Mouza, J.D. (2018) Predicting Blast Fragmentation Efficiency Using Discriminant Analysis. In: Franklin, J.A., Ed., *Measurement of Blast Fragmentation*, Routledge, 203-207. https://doi.org/10.1201/9780203747919-29

[14] Chung, S.H. and Katsabanis, P.D. (2000) Fragmentation Prediction Using Improved Engineering Formulae. *Fragblast*, **4**, 198-207. https://doi.org/10.1076/frag.4.3.198.7392

[15] Hamdi, E., Du Mouza, J. and Alain, F.J. (2002) Influence of Rock Mass Structure on Blast Efficiency. *Proceedings of the 7th International Symposium on Rock Fragmentation*, Beijing, 11-15 August 2002, 1-12.

[16] Cunningham, C.V.B. (2005) The Kuz-Ram Fragmentation Model—20 Years on. *Brighton Conference Proceedings*, Brighton, 13-16 September 2005, 201-210.

[17] Gheibie, S., Aghababaei, H., Hoseinie, S.H. and Pourrahimian, Y. (2009) Modified Kuz-Ram Fragmentation Model and Its Use at the Sungun Copper Mine. *International Journal of Rock Mechanics and Mining Sciences*, **46**, 967-973. https://doi.org/10.1016/j.ijrmms.2009.05.003

[18] Cunningham, C.V.B. (1983) The Kuz-Ram Model for Prediction of Fragmentation from Blasting. *Proceedings of the First International Symposium on Rock Fragmentation by Blasting*, Sweden, 23-26 August 1983, 439-453. https://cir.nii.ac.jp/crid/1573387449354221568

[19] Cunningham, C.V.B. (1987) Fragmentation Estimations and the Kuz-Ram Model-Four Years on. *Proceedings of the Second International Symposium on Rock Fragmentation by Blasting*, Keystone, 23-26 August 1987, 475-478.

[20] Lawal, A.I. (2021) A New Modification to the Kuz-Ram Model Using the Fragment Size Predicted by Image Analysis. *International Journal of Rock Mechanics and Mining Sciences*, **138**, Article ID: 104595. https://doi.org/10.1016/j.ijrmms.2020.104595

[21] Djordjevic, N. (1999) A Two-Component Model of Blast Fragmentation. *AusIMM Proceedings*, Kalgoorlie, 7-11 November 1999, 9-13.

[22] Onederra, I., Esen, S. and Jankovic, A. (2004) Estimation of Fines Generated by Blasting—Applications for the Mining and Quarrying Industries. *Mining Technology*,

113, 237-247. https://doi.org/10.1179/037178404225006191

[23] Ouchterlony, F. (2005) The Swebrec© Function: Linking Fragmentation by Blasting and Crushing. *Mining Technology*, **114**, 29-44. https://doi.org/10.1179/037178405x44539

[24] Ouchterlony, F. and Moser, P. (2006) Likenesses and Differences in the Fragmentation of Full-Scale and Model-Scale Blasts. *International Symposium on Rock Fragmentation by Blasting*, Santiago, 7-11 May 2006, 207-220.

[25] Ouchterlony, F. and Moser, P. (2006) Die Swebrec-Funktion: Eine neue Korngrößenverteilungsfunktion und ihr praktischer Einsatz in der Sprengtechnik. *BHM Berg- und Hüttenmännische Monatshefte*, **151**, 389-404. https://doi.org/10.1007/bf03165378

[26] Ouchterlony, F., Sanchidrián, J.A. and Moser, P. (2016) Percentile Fragment Size Predictions for Blasted Rock and the Fragmentation-Energy Fan. *Rock Mechanics and Rock Engineering*, **50**, 751-779. https://doi.org/10.1007/s00603-016-1094-x

[27] Ouchterlony, F. and Sanchidrián, J.A. (2018) A Review of the Development of Better Prediction Equations for Blast Fragmentation. *Rock Dynamics and Applications*, **3**, 25-45.

[28] Sanchidrián, J.A., Ouchterlony, F., Segarra, P. and Moser, P. (2014) Size Distribution Functions for Rock Fragments. *International Journal of Rock Mechanics and Mining Sciences*, **71**, 381-394. https://doi.org/10.1016/j.ijrmms.2014.08.007

[29] Kuznetsov, V.M. (1973) The Mean Diameter of the Fragments Formed by Blasting Rock. **9**, 144-148. https://doi.org/10.1007/bf02506177

[30] Monjezi, M., Amiri, H., Farrokhi, A. and Goshtasbi, K. (2010) Prediction of Rock Fragmentation Due to Blasting in Sarcheshmeh Copper Mine Using Artificial Neural Networks. *Geotechnical and Geological Engineering*, **28**, 423-430. https://doi.org/10.1007/s10706-010-9302-z

[31] Monjezi, M., Rezaei, M. and Yazdian Varjani, A. (2009) Prediction of Rock Fragmentation Due to Blasting in Gol-E-Gohar Iron Mine Using Fuzzy Logic. *International Journal of Rock Mechanics and Mining Sciences*, **46**, 1273-1280. https://doi.org/10.1016/j.ijrmms.2009.05.005

[32] Sayadi, A., Monjezi, M., Talebi, N. and Khandelwal, M. (2013) A Comparative Study on the Application of Various Artificial Neural Networks to Simultaneous Prediction of Rock Fragmentation and Backbreak. *Journal of Rock Mechanics and Geotechnical Engineering*, **5**, 318-324. https://doi.org/10.1016/j.jrmge.2013.05.007

[33] Zhang, Z.X., Sanchidrián, J.A., Ouchterlony, F. and Luukkanen, S. (2022) Reduction of Fragment Size from Mining to Mineral Processing: A Review. *Rock Mechanics and Rock Engineering*, **56**, 747-778. https://doi.org/10.1007/s00603-022-03068-3

[34] Zhang, W., Zhang, Y., Gu, X., Wu, C. and Han, L. (2021) Application of Soft Computing, Machine Learning, Deep Learning and Optimizations in Geoengineering and Geoscience. Springer. https://doi.org/10.1007/978-981-16-6835-7

[35] Raina, A.K., Vajre, R., Sangode, A. and Ram Chandar, K. (2024) Application of Artificial Intelligence in Predicting Rock Fragmentation: A Review. In: Nguyen, H., Bui, X.N., *et al*., Eds., *Applications of Artificial Intelligence in Mining, Geotechnical and Geoengineering*, Elsevier, 291-314. https://doi.org/10.1016/b978-0-443-18764-3.00003-5

[36] Sharma, M., Choudhary, B.S., Raina, A.K., Khandelwal, M. and Rukhiyar, S. (2024) Prediction of Rock Fragmentation in a Fiery Seam of an Open-Pit Coal Mine in India. *Journal of Rock Mechanics and Geotechnical Engineering*, **16**, 2879-2893.

https://doi.org/10.1016/j.jrmge.2023.11.047

[37] Feng, X.T., Yang, C.X., He, B.G., Yao, Z.B., Hu, L., Zhang, W., *et al*. (2024) Artificial Intelligence Technology in Rock Mechanics and Rock Engineering. *Deep Resources Engineering*, **1**, Article ID: 100008. https://doi.org/10.1016/j.deepre.2024.100008

[38] Choi, Y., Nguyen, H., Bui, X.N., Nguyen-Thoi, T. and Park, S. (2020) Estimating Ore Production in Open-Pit Mines Using Various Machine Learning Algorithms Based on a Truck-Haulage System and Support of Internet of Things. *Natural Resources Research*, **30**, 1141-1173. https://doi.org/10.1007/s11053-020-09766-5

[39] He, B., Armaghani, D.J., Lai, S.H. and Mohamad, E.T. (2024) Application of an Expert Extreme Gradient Boosting Model to Predict Blast-Induced Air-Overpressure in Quarry Mines. In: Nguyen, H., Bui, X.N., *et al*., Eds., *Applications of Artificial Intelligence in Mining, Geotechnical and Geoengineering*, Elsevier, 269-289. https://doi.org/10.1016/b978-0-443-18764-3.00019-9

[40] Arthur, C.K., Temeng, V.A. and Ziggah, Y.Y. (2019) Soft Computing-Based Technique as a Predictive Tool to Estimate Blast-Induced Ground Vibration. *Journal of Sustainable Mining*, **18**, 287-296. https://doi.org/10.1016/j.jsm.2019.10.001

[41] Martinsen, M., Fentaye, A.D., Dahlquist, E. and Zhou, Y. (2023) Holistic Approach Promotes Failure Prevention of Smart Mining Machines Based on Bayesian Networks. *Machines*, **11**, Article 940. https://doi.org/10.3390/machines11100940

[42] Ativor, G., Temeng, V.A. and Ziggah, Y.Y. (2024) Predicting Abrasive Wear in Excavator Bucket Teeth Using Cutting-Edge Vector Machines and Artificial Neural Networks. *Ghana Mining Journal*, **24**, 92-106. https://journals.umat.edu.gh/index.php/gmj/article/view/721

[43] Ji, S., Li, W., Zhang, B., Zhou, L. and Duan, C. (2021) Bucket Teeth Detection Based on Faster Region Convolutional Neural Network. *IEEE Access*, **9**, 17649-17661. https://doi.org/10.1109/access.2021.3054436

[44] Gao, W., Karbasi, M., Hasanipanah, M., Zhang, X. and Guo, J. (2017) Developing GPR Model for Forecasting the Rock Fragmentation in Surface Mines. *Engineering with Computers*, **34**, 339-345. https://doi.org/10.1007/s00366-017-0544-8

[45] Gebretsadik, A., Kumar, R., Fissha, Y., Kide, Y., Okada, N., Ikeda, H., *et al*. (2024) Enhancing Rock Fragmentation Assessment in Mine Blasting through Machine Learning Algorithms: A Practical Approach. *Discover Applied Sciences*, **6**, Article No. 223. https://doi.org/10.1007/s42452-024-05888-0

[46] Ke, B., Nguyen, H., Bui, X.N. and Costache, R. (2021) Estimation of Ground Vibration Intensity Induced by Mine Blasting Using a State-of-the-Art Hybrid Autoencoder Neural Network and Support Vector Regression Model. *Natural Resources Research*, **30**, 3853-3864. https://doi.org/10.1007/s11053-021-09890-w

[47] Zhao, G., Wang, M. and Liang, W. (2022) A Comparative Study of SSA-BPNN, SSA-ENN, and SSA-SVR Models for Predicting the Thickness of an Excavation Damaged Zone around the Roadway in Rock. *Mathematics*, **10**, Article 1351. https://doi.org/10.3390/math10081351

[48] Cui, K. and Jing, X. (2018) Research on Prediction Model of Geotechnical Parameters Based on BP Neural Network. *Neural Computing and Applications*, **31**, 8205-8215. https://doi.org/10.1007/s00521-018-3902-6

[49] Amoako, R., Jha, A. and Zhong, S. (2022) Rock Fragmentation Prediction Using an Artificial Neural Network and Support Vector Regression Hybrid Approach. *Mining*, **2**, 233-247. https://doi.org/10.3390/mining2020013

[50] Bejani, M.M. and Ghatee, M. (2021) A Systematic Review on Overfitting Control in

Shallow and Deep Neural Networks. *Artificial Intelligence Review*, **54**, 6391-6438. https://doi.org/10.1007/s10462-021-09975-1

[51] Tharwat, A. (2019) Parameter Investigation of Support Vector Machine Classifier with Kernel Functions. *Knowledge and Information Systems*, **61**, 1269-1302. https://doi.org/10.1007/s10115-019-01335-4

[52] Trojovska, E., Dehghani, M. and Trojovsky, P. (2022) Zebra Optimization Algorithm: A New Bio-Inspired Optimization Algorithm for Solving Optimization Algorithm. *IEEE Access*, **10**, 49445-49473. https://doi.org/10.1109/access.2022.3172789

[53] Mirjalili, S., Mirjalili, S.M. and Lewis, A. (2014) Grey Wolf Optimizer. *Advances in Engineering Software*, **69**, 46-61. https://doi.org/10.1016/j.advengsoft.2013.12.007

[54] Frazier, P.I. (2018) A Tutorial on Bayesian Optimization. arXiv: 1807.02811.

[55] Yu, Z., Du, L.F., Liu, J.X., Zhou, J. and Li, C.Q. (2025) Feasibility of a Hybrid AHA-GPR Model for Predicting Blasting Fragmention in Surface Mines. *Earth Science Informatics*, **18**, Article No. 278. https://doi.org/10.1007/s12145-025-01817-w

[56] Zhao, J., Li, D., Zhou, J., Armaghani, D.J. and Zhou, A. (2024) Performance Evaluation of Rock Fragmentation Prediction Based on RF-BOA, AdaBoost-BOA, GBoost-BOA, and ERT-BOA Hybrid Models. *Deep Underground Science and Engineering*, **4**, 3-17. https://doi.org/10.1002/dug2.12089

[57] Zheng, H., Liu, J., Zhuang, R., Zhao, F., Zhen, M., Wang, Y., *et al.* (2023) Enhancing the Performance of LSSVM Model in Predicting Rock Fragmentation Size via Optimization Algorithms. *KSCE Journal of Civil Engineering*, **27**, 3765-3777. https://doi.org/10.1007/s12205-023-1327-y

[58] Yari, M., He, B., Armaghani, D.J., Abbasi, P. and Mohamad, E.T. (2023) A Novel Ensemble Machine Learning Model to Predict Mine Blasting-Induced Rock Fragmentation. *Bulletin of Engineering Geology and the Environment*, **82**, Article No. 187. https://doi.org/10.1007/s10064-023-03138-y

[59] Huang, J., Asteris, P.G., Manafi Khajeh Pasha, S., Mohammed, A.S. and Hasanipanah, M. (2020) A New Auto-Tuning Model for Predicting the Rock Fragmentation: A Cat Swarm Optimization Algorithm. *Engineering with Computers*, **38**, 2209-2220. https://doi.org/10.1007/s00366-020-01207-4

[60] Fang, Q., Nguyen, H., Bui, X., Nguyen-Thoi, T. and Zhou, J. (2020) Modeling of Rock Fragmentation by Firefly Optimization Algorithm and Boosted Generalized Additive Model. *Neural Computing and Applications*, **33**, 3503-3519. https://doi.org/10.1007/s00521-020-05197-8

[61] Zhou, J., Li, C., Arslan, C.A., Hasanipanah, M. and Bakhshandeh Amnieh, H. (2019) Performance Evaluation of Hybrid FFA-ANFIS and GA-ANFIS Models to Predict Particle Size Distribution of a Muck-Pile after Blasting. *Engineering with Computers*, **37**, 265-274. https://doi.org/10.1007/s00366-019-00822-0

[62] Hasanipanah, M., Amnieh, H.B., Arab, H. and Zamzam, M.S. (2016) Feasibility of PSO-ANFIS Model to Estimate Rock Fragmentation Produced by Mine Blasting. *Neural Computing and Applications*, **30**, 1015-1024. https://doi.org/10.1007/s00521-016-2746-1

[63] Murlidhar, B.R., Armaghani, D.J., Mohamad, E.T. and Changthan, S. (2018) Rock Fragmentation Prediction through a New Hybrid Model Based on Imperial Competitive Algorithm and Neural Network. *Smart Construction Research*, **2**, 1-12.

[64] Ebrahimi, E., Monjezi, M., Khalesi, M.R. and Armaghani, D.J. (2015) Prediction and Optimization of Back-Break and Rock Fragmentation Using an Artificial Neural Network and a Bee Colony Algorithm. *Bulletin of Engineering Geology and the Environ-*

ment, **75**, 27-36. https://doi.org/10.1007/s10064-015-0720-2

[65] Eshun, P.A. and Dzigbordi, K.A. (2016) Control of Ore Loss and Dilution at Anglogold Ashanti, Iduapriem Mine Using Blast Movement Monitoring System. *Ghana Mining Journal*, **16**, 49-59. https://doi.org/10.4314/gm.v16i1.6

[66] Wright, L.G., Onodera, T., Stein, M.M., Wang, T., Schachter, D.T., Hu, Z., *et al*. (2022) Deep Physical Neural Networks Trained with Backpropagation. *Nature*, **601**, 549-555. https://doi.org/10.1038/s41586-021-04223-6

[67] Hecht-Nielsen, R. (1992) Theory of the Backpropagation Neural Network. In: Wechsler, H., Ed., *Neural Networks for Perception*, Academic Press, 65-93.

[68] Ativor, G., Eshun, S.N., Otchere, P.K. and Ziggah, Y.Y. (2026) A Hybrid Metaheuristic-Machine Learning Framework for High-Fidelity Prediction of Geopolymer Concrete Compressive Strength. *Journal of Building Pathology and Rehabilitation*, **11**, Article No. 106. https://doi.org/10.1007/s41024-026-00786-x

[69] Yoon, H., Jun, S.C., Hyun, Y., Bae, G.O. and Lee, K.K. (2011) A Comparative Study of Artificial Neural Networks and Support Vector Machines for Predicting Groundwater Levels in a Coastal Aquifer. *Journal of Hydrology*, **396**, 128-138. https://doi.org/10.1016/j.jhydrol.2010.11.002

[70] Jain, A.K., Jianchang Mao, and Mohiuddin, K.M. (1996) Artificial Neural Networks: A Tutorial. *Computer*, **29**, 31-44. https://doi.org/10.1109/2.485891

[71] Zhang, F. and O'Donnell, L.J. (2020) Support Vector Regression. In: Mechelli, A. and Vieira, S., Eds., *Machine Learning*, Elsevier, 123-140. https://doi.org/10.1016/b978-0-12-815739-8.00007-9

[72] Shin, H. and Cho, S. (2006) Response Modeling with Support Vector Machines. *Expert Systems with Applications*, **30**, 746-760. https://doi.org/10.1016/j.eswa.2005.07.037

[73] Loki, M., Mindila, A. and Cheruiyot, W. (2024) Hyper-Parameter Optimization of Kernel Functions on Multi-Class Text Categorization: A Comparative Evaluation. *WIREs Data Mining and Knowledge Discovery*, **15**, e1572. https://doi.org/10.1002/widm.1572

[74] Faris, H., Aljarah, I., Al-Betar, M.A. and Mirjalili, S. (2017) Grey Wolf Optimizer: A Review of Recent Variants and Applications. *Neural Computing and Applications*, **30**, 413-435. https://doi.org/10.1007/s00521-017-3272-5

[75] Pelikan, M. (2005) Bayesian Optimization Algorithm. In: Pelikan, M., Ed., *Hierarchical Bayesian Optimization Algorithm*, Springer, 31-48. https://doi.org/10.1007/978-3-540-32373-0_3

[76] Pelikan, M., Sastry, K. and Goldberg, D.E. (2002) Scalability of the Bayesian Optimization Algorithm. *International Journal of Approximate Reasoning*, **31**, 221-258. https://doi.org/10.1016/s0888-613x(02)00095-6

[77] Ativor, G., Ziggah, Y.Y. and Temeng, V.A. (2025) A Novel Intelligent Approach for Predicting Wear of Excavator Bucket Teeth Based on Hybrid ICA-XGBoost Model. engrXiv. https://doi.org/10.31224/4581

[78] Kannangara, K.K.P.M., Zhou, W., Ding, Z. and Hong, Z. (2022) Investigation of Feature Contribution to Shield Tunneling-Induced Settlement Using Shapley Additive Explanations Method. *Journal of Rock Mechanics and Geotechnical Engineering*, **14**, 1052-1063. https://doi.org/10.1016/j.jrmge.2022.01.002

[79] Karunasingha, D.S.K. (2022) Root Mean Square Error or Mean Absolute Error? Use Their Ratio as Well. *Information Sciences*, **585**, 609-629. https://doi.org/10.1016/j.ins.2021.11.036

[80] Ativor, G., Temeng, V.A. and Ziggah, Y.Y. (2025) Optimisation of Multilayer Perceptron Neural Network Using Five Novel Metaheuristic Algorithms for the Prediction of Wear of Excavator Bucket Teeth. *Knowledge-Based Systems*, **321**, Article ID: 113753. https://doi.org/10.1016/j.knosys.2025.113753

[81] Akoglu, H. (2018) User's Guide to Correlation Coefficients. *Turkish Journal of Emergency Medicine*, **18**, 91-93. https://doi.org/10.1016/j.tjem.2018.08.001